JOURNAL OF AIRCRAFT
Vol. 45, No. 2, March–April 2008

Conceptual Study of Gondola Stabilization in a Balloon System

Joshua Ashenberg*
Harvard–Smithsonian Center for Astrophysics, Cambridge, Massachusetts 02138

DOI: 10.2514/1.29710

Pointing stabilization of a gondola carried by a stratospheric balloon is a challenging problem due to upper atmospheric winds and due to the multibody nature of the balloon system. The gondola provides a platform for a scientific experiment that requires point stabilization. The experiment apparatus is inside a capsule attached to the gondola base. The proposed actuator is a displacement mechanism that moves the capsule along the gondola base. The current paper presents a feasibility study of this concept. The flight dynamic model of the balloon system is formulated and analyzed, and a preliminary investigation of feasible control logic is presented and tested.

Nomenclature

$\mathbf{A}$	=	system matrix
$\mathbf{B}$	=	control matrix
b	=	length
$\mathbf{C}_{ba}$	=	rotation matrix ($a \rightarrow b$)
C_D	=	drag coefficient
D	=	drag
d	=	length
$\mathbf{F}$	=	force
g	=	gravity acceleration
I	=	moment of inertia
I_δ	=	controller input
K	=	kinetic energy
$\mathbf{K}$	=	stiffness matrix
L_*	=	length
$\mathbf{M}$	=	mass matrix
m_*	=	mass
n	=	surface normal direction
p	=	roll rate
q	=	pitch rate
$\mathbf{R}$	=	control weight matrix
$\Re_*$	=	vectrix
r	=	yaw rate
$\mathbf{S}$	=	state weight matrix
$\mathbf{T}$	=	torque
t	=	time
U	=	potential energy
$\mathbf{u}$	=	control vector
$\mathbf{V}$	=	velocity
$\mathbf{W}$	=	wind velocity
$\mathbf{X}$	=	state vector
X_I	=	balloon inertial coordinate
Y_I	=	balloon inertial coordinate
Z_I	=	balloon inertial coordinate
δ	=	control displacement
θ	=	pitch angle
ρ_a	=	air density
ρ_*	=	length
ϕ	=	roll angle
ψ	=	yaw angle
ω	=	angular velocity
$\omega^\times$	=	angular velocity matrix

Subscripts

B	=	balloon
C	=	capsule
G	=	gondola
P	=	payload
T	=	tether
$*$	=	wild card

Superscripts

A/B	=	subscript A relative to subscript B
$\cdot$	=	time derivative in the inertial frame
$^\circ$	=	time derivative in the local frame

Introduction

THE presented problem is motivated by an experiment for testing the principle of equivalence in general relativity [1–3]. In this experiment, an evacuated capsule is released from a stratospheric balloon at an altitude of 40 km. A cofalling spinning detector inside the capsule contains two proof masses and an extremely accurate measurement system. Tight drop conditions are required: the capsule orientation should be vertical with minimal angular rate. Attaining these conditions is quite demanding, given the atmospheric winds and gravity waves at that high altitude. In addition to these disturbances, the balloon system (Fig. 1) is excited by its neutral buoyancy oscillations. It is convenient to denote the main modes of oscillations by bob, rotation, and swing (the vertical buoyant oscillations, the yaw, and the pendular motion of the payload, respectively). Obviously, passive stabilization is unfeasible and active stabilization of the complete system is impractical. Although the swing can be partially reduced by a damping mechanism and the rotation can be regulated, attitude control of the gondola remains a challenging task. Recall that we seek stabilization of the payload rather than the whole system. Accordingly, one feasible approach is to use reaction wheels [4]. This technique may have some drawbacks and additional complications from the required thrusters for desaturating the wheels. Another efficient, robust, and cost-effective method was applied for pointing stabilization of artificial satellites. The idea was to attach a tether with a ballast at its far end. The tether produces a strong torque about the pitch and roll axes via its tension, thereby augmenting the gravity gradient stabilization. A further step is to move the attachment point along a surface, typically perpendicular to the yaw axis, in discrete steps using a stepper motor. This mechanism is desirable and effective for disturbance rejection. Furthermore, it can be shown [5] that the energy required by the stepper motor is far less than the energy consumed by other actuators. This method was applied successfully by the author [6] for pointing control under internal periodic excitations due to the eccentricity in elliptic orbits. The resemblance of a gondola attached by a tether suggests a similar concept in which internal disturbances also exist but now come from the balloon dynamics. In the current design, the

Received 11 January 2007; revision received 10 July 2007; accepted for publication 10 July 2007. Copyright © 2007 by the American Institute of Aeronautics and Astronautics, Inc. All rights reserved. Copies of this paper may be made for personal or internal use, on condition that the copier pay the $10.00 per-copy fee to the Copyright Clearance Center, Inc., 222 Rosewood Drive, Danvers, MA 01923; include the code 0021-8669/08 $10.00 in correspondence with the CCC.

*Radio and Geoastronomy Division, 60 Garden Street, Mail Stop 80. Senior Member AIAA.

stepper motor is attached to the gondola and moves the capsule in two dimensions. Notice that the rigging point is fixed; thus, although the stabilization mechanics are different from tether stabilization, the concept is similar.

There are two rigid design requirements. At the drop epoch, the capsule angular deviation and its angular rate should be less than 0.5 and 0.1 deg/s, respectively. Also, the control displacement and the control displacement rate are limited to 0.2 and 0.1 m/s, respectively. All other states of this system are unconstrained, although it is obvious that some state variables should be limited.

The final goal of this work is stabilizing the capsule. Therefore, loosely speaking, the other bodies can be viewed as a part of the disturbance mechanism; it is expected that a successful stabilization mechanism will work well with a slightly different system and with different disturbances. Consequently, it will be assumed that the system can be modeled by a simple discretization to four bodies: a spherical balloon, tether, gondola, and capsule. All bodies are considered rigid, including the massless tether, and are symbolically connected by spherical joints. There is an option to add a dissipation mechanism via a water tank attached to the balloon. The atmosphere is standard and the atmospheric disturbances are acting through density gradients, typical winds, and gravity waves. It is further assumed that the variations of the balloon's physical parameters are slow relative to the system dynamics and thus can be ignored. The only object perturbed by the atmospheric forces is the balloon; the other objects' dynamics are dictated by the multibody constraints.

The bodies are represented by B for the balloon, T for the tether, G for the gondola, C for the capsule, and D for the payload. C is also interchangeable with control, because the capsule can be considered as a controller. There are four right-hand coordinate reference frames: inertial, balloon, tether, and payload (the payload consists of gondola and capsule). The attitude kinematics is formulated by using vectrix algebra [7]. The basic symbol is the vectrix $\Re_a = [\mathbf{a}_1 \ \ \mathbf{a}_2 \ \ \mathbf{a}_3]^T$, where $\mathbf{a}_i$ are the base vectors for the frame of reference $\Re_a$. A vector $\mathbf{v}$ is expressed in terms of its column vector in $\Re_a$ as $\mathbf{v} = \{v\}^T \Re_a$. The column vector is the projection (or representation) of a vector on a particular reference frame, $\{v\} = \Re_a \cdot \mathbf{v}$. Vectrix notation and vectrix algebra are convenient for multiple reference frames, because a vector is independent of a particular reference frame. The rotation sequences with Euler angles are as follows. The balloon uses $1 \to 2 \to 3$, the tether uses $2 \to 1$, and the payload uses $3 \to 2 \to 1$. All geometrical parameters are defined by Figs. 1 and 2. The standard roll, pitch, and yaw angles are denoted by ϕ, θ, and ψ; the corresponding rates are p, q, and r; and $\boldsymbol{\omega}^\times$ represents the angular velocity matrix (an operator)

$$\boldsymbol{\omega}^\times \equiv \begin{bmatrix} 0 & -\omega_3 & \omega_2 \\ \omega_3 & 0 & -\omega_1 \\ -\omega_2 & \omega_1 & 0 \end{bmatrix}$$

(The rotation matrix rate, with $\boldsymbol{\omega}^\times$ terminology, is $\dot{\mathbf{C}} = -\boldsymbol{\omega}^\times \mathbf{C}$.) Additional assumptions and notations will be specified later.

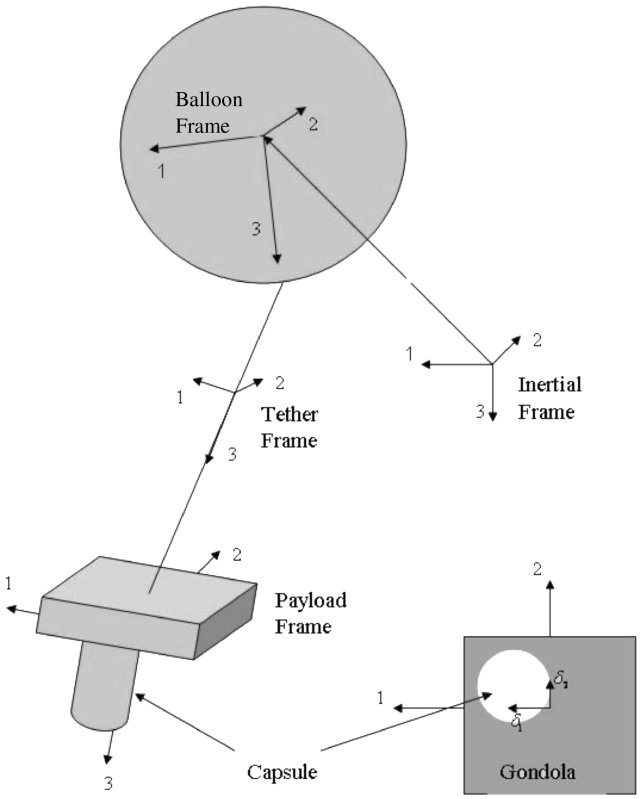

Fig. 1 Schematic of the balloon system.

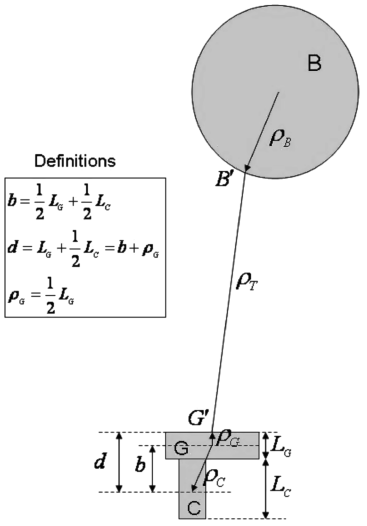

Fig. 2 Geometrical definitions.

Dynamic Model

Derivation of the Equations of Motion

Let us first consider the basic autonomous system in which the capsule is fixed to the gondola. The balloon center is taken as the root of the kinematical tree. We assume further that the tether's restoring twist torque is negligible; thus, the tether yaw has no dynamics. Consequently, the distribution of the degrees of freedom is as follows. The balloon has three translations (two horizontals and a vertical) and three rotations (roll, pitch, and yaw), the tether has two rotations (roll and pitch), and the payload has three rotations (roll, pitch, and yaw). Accordingly, the autonomous system dynamics consists of 11 degrees of freedom.

It is convenient to augment the system state by adding the control displacements (δ_1, δ_2). Alternatively, (δ_1, δ_2) could be considered as control variables. But notice that the actuator (the capsule) is quite massive compared with typical aircraft actuators. Consequently, the control accelerations $(\ddot{\delta}_1, \ddot{\delta}_2)$ are expected to appear in the equations of motion. These accelerations should be modeled or considered as external disturbances. Accordingly, the better approach is to consider (δ_1, δ_2) as intrinsic state variables. The natural and simplest model is to assume a linearity between an input control (torque or electrical power) and the capsule acceleration:

$$\frac{\mathrm{d}^2 \delta_j}{\mathrm{d}t^2} = K_\delta I_{\delta_j} \qquad j = 1, 2 \tag{1}$$

The gain K_δ depends on the step-motor characteristics and on the capsule mass. With reference to Fig. 2, it is straightforward to proceed with the kinematical modeling, using the following vectrix geometry:

$$\boldsymbol{\rho}_B = \Re_B^T \begin{pmatrix} 0 \\ 0 \\ \rho_B \end{pmatrix}, \qquad \boldsymbol{\rho}_T = \Re_T^T \begin{pmatrix} 0 \\ 0 \\ L \end{pmatrix}$$
$$\boldsymbol{\rho}_G = \Re_P^T \begin{pmatrix} 0 \\ 0 \\ -\rho_G \end{pmatrix}, \qquad \boldsymbol{\rho}_C = \Re_C^T \begin{pmatrix} \delta_1 \\ \delta_2 \\ b \end{pmatrix} \tag{2}$$

The rotation matrices are constructed by the particular rotations. The angular velocities are computed directly from the rotation matrices using the angular rotation operator $\boldsymbol{\omega}^{\times} = -\dot{\mathbf{C}}\mathbf{C}^T$. The rotations and the rates for the balloon, tether, and payload are shown next:

$$\mathbf{C}_{BI} = \begin{bmatrix} c\theta c\psi & s\phi s\theta c\psi + c\phi s\psi & -c\phi s\theta c\psi + s\phi s\psi \\ -c\theta s\psi & -s\phi s\theta s\psi + c\phi c\psi & c\phi s\theta s\psi + s\phi c\psi \\ s\theta & -s\phi c\theta & c\phi c\theta \end{bmatrix}_{(B)} \tag{3a}$$

$$\mathbf{C}_{TI} = \begin{bmatrix} c\theta & 0 & -s\theta \\ s\phi s\theta & c\phi & s\phi c\theta \\ c\phi s\theta & -s\phi & c\phi c\theta \end{bmatrix}_{(T)} \tag{3b}$$

$$\mathbf{C}_{PI} = \begin{bmatrix} c\theta c\psi & c\theta s\psi & -s\theta \\ s\phi s\theta c\psi - c\phi s\psi & s\phi s\theta s\psi + c\phi c\psi & s\phi s\theta \\ c\phi s\theta c\psi + s\phi s\psi & c\phi s\theta s\psi - s\phi c\psi & c\phi c\theta \end{bmatrix}_{(P)} \tag{3c}$$

$$\begin{bmatrix} p \\ q \\ r \end{bmatrix}_{(B)} = \begin{bmatrix} c\theta c\psi & s\psi & 0 \\ -c\theta s\psi & c\psi & 0 \\ s\theta & 0 & 1 \end{bmatrix} \begin{bmatrix} \dot{\varphi} \\ \dot{\theta} \\ \dot{\psi} \end{bmatrix}_{(B)} \tag{4a}$$

$$\begin{bmatrix} p \\ q \\ r \end{bmatrix}_{(T)} = \begin{bmatrix} 1 & 0 & 0 \\ 0 & c\phi & 0 \\ 0 & -s\phi & 0 \end{bmatrix} \begin{bmatrix} \dot{\varphi} \\ \dot{\theta} \\ 0 \end{bmatrix}_{(T)} \tag{4b}$$

$$\begin{bmatrix} p \\ q \\ r \end{bmatrix}_{(P)} = \begin{bmatrix} 1 & 0 & -s\theta \\ 0 & c\phi & s\phi c\theta \\ 0 & -s\phi & c\phi c\theta \end{bmatrix} \begin{bmatrix} \dot{\varphi} \\ \dot{\theta} \\ \dot{\psi} \end{bmatrix}_{(P)} \tag{4c}$$

Formulating the equations of motion is now a straightforward task, and we will choose the Lagrange method. By eliminating the constraints, the Lagrangian is suitable for multibody dynamics. Recall that the Lagrangian formulation is

$$\frac{\mathrm{d}}{\mathrm{d}t}\left(\frac{\partial T}{\partial \dot{q}_i}\right) - \frac{\partial T}{\partial q_i} + \frac{\partial V}{\partial q} = \mathbf{Q}_i \tag{5}$$

where the generalized force $\mathbf{Q}_i$ (for state i) is related to the aerodynamic force $\mathbf{F}^k$ and to the torque $\mathbf{T}^k$ acting on each k body:

$$\mathbf{Q}_i = \sum_k \mathbf{F}^k \cdot \frac{\partial \dot{\mathbf{R}}_k}{\partial \dot{q}_i} + \sum_k \mathbf{T}^k \cdot \frac{\partial \boldsymbol{\omega}_k}{\partial \dot{q}_i} \tag{6}$$

The state X is now of order 26 [states (12, 13) and (25, 26) are the capsule displacements and their rates]:

$$\mathbf{X} = [X_I, Y_I, Z_I, \varphi_B, \theta_B, \psi_B, \phi_T, \theta_T, \phi_P, \theta_P, \psi_P, \delta_1, \delta_2, \dot{X}_I, \dot{Y}_I, \dot{Z}_I, \dot{\phi}_B, \dot{\theta}_B, \dot{\psi}_B, \dot{\phi}_T, \dot{\theta}_T, \dot{\phi}_P, \dot{\theta}_P, \dot{\psi}_P, \dot{\delta}_1, \dot{\delta}] \tag{7}$$

Before proceeding with the Lagrangian formulation, let us consider a special type of aerodynamic force related to the so-called virtual mass [8]. It reflects the inertia of the surrounding fluid. Given the hydrodynamic potential Φ, the virtual mass tensor depends on the body shape as follows [8]:

$$m_{ij} = -\oiint_{\text{surface}} \rho_a \Phi_i n_j \, \mathrm{d}S \tag{8}$$

In general, a 3 by 3 virtual mass matrix [9] is required for airship aerodynamics. Because the balloon is approximated as a sphere, the virtual mass is simply [8]

$$m_a \equiv m_{11} = m_{22} = m_{33} = \tfrac{2}{3}\pi R^3 \rho_a \equiv \tfrac{1}{2} m_{\text{air}} \tag{9}$$

Now, having the virtual mass, the system mass distribution, and its kinematics, the kinetic energy can be formulated as follows:

$$K = \tfrac{1}{2}(m_B + m_a)V_B^2 + \tfrac{1}{2}m_G V_G^2 + \tfrac{1}{2}m_C V_C^2 + \tfrac{1}{2}\boldsymbol{\omega}_B \cdot (\mathbf{I}^B + \mathbf{I}^a) \cdot \boldsymbol{\omega}_B + \tfrac{1}{2}\boldsymbol{\omega}_P \cdot (\mathbf{I}^G + \mathbf{I}^C) \cdot \boldsymbol{\omega}_P \tag{10}$$

where $\mathbf{I}^B \equiv \mathrm{diag}(I_B, I_B, I_B)$, $\mathbf{I}^G = \mathrm{diag}(I_{xx}^G, I_{yy}^G, I_{zz}^G)$, and $\mathbf{I}^C = \mathrm{diag}(I_t^C, I_t^C, I_a^C)$.

I^a reflects the rotational properties of the virtual mass tensor. It is null for a spherical balloon and appears in the energy equation (10), for formality. The velocity chain for the three massive bodies, starting from the balloon center, is

$$\mathbf{V}_B = \Re_I^T \begin{pmatrix} \dot{X}_I \\ \dot{Y}_I \\ \dot{Z}_I \end{pmatrix} \tag{11a}$$

$$\mathbf{V}_G = \Re_I^T (\{V_B\} + \mathbf{C}_{IB}\boldsymbol{\omega}_B^{\times}\{\rho_B\} + \mathbf{C}_{IT}\boldsymbol{\omega}_T^{\times}\{\rho_T\} - \mathbf{C}_{IP}\boldsymbol{\omega}_P^{\times}\{\rho_G\}) \tag{11b}$$

$$\mathbf{V}_C = \Re_I^T (\{V_B\} + \mathbf{C}_{IB}\boldsymbol{\omega}_B^{\times}\{\rho_B\} + \mathbf{C}_{IT}\boldsymbol{\omega}_T^{\times}\{\rho_T\} + \mathbf{C}_{IP}\boldsymbol{\omega}_P^{\times}\{\rho_{G'C}\} + \mathbf{C}_{IP}\{\mathring{\rho}_C\}) \tag{11c}$$

Notice that $\mathring{\rho}_C$ is a time derivative in $\Re_C$ (and $\dot{\rho}$ is a time derivative in $\Re_I$).

It is easy to see from Fig. 2 that the potential energy takes on the form

$$U = \Big[-m_B Z_I - m_G\Big(Z_I + \{\mathbf{C}_{IB}\{\rho_B\}\}_3 - \rho_B + \{\mathbf{C}_{IT}\{\rho_T\}\}_3 - L - \{\mathbf{C}_{IP}\{\rho_G\}\}_3 - \tfrac{1}{2}L_C\Big) - m_C(Z_I + \{\mathbf{C}_{IB}\{\rho_B\}\}_3 - \rho_B + \{\mathbf{C}_{IT}\{\rho_T\}\}_3 - L + \mathbf{C}_{IP}\{\rho_{G'C}\} - d)\Big]g \tag{12}$$

Next, let us consider the applied force. Recall that the aerodynamic force due to the virtual mass is already an intrinsic part of the system dynamics. The other aerodynamic force is due to viscous drag acting on a sphere:

$$\mathbf{D} = -\tfrac{1}{2}\rho_a C_D S_B \mathbf{W}_{\text{rel}} |\mathbf{W}_{\text{rel}}| \tag{13}$$

where ρ_a is the atmospheric density at altitude H, C_D is the drag coefficient that depends on Reynolds number ($C_D \approx 0.5$), S_B is the

balloon cross-sectional area, and $\mathbf{W}_{\text{rel}}$ is the relative velocity between the balloon and the wind $\mathbf{W}$:

$$\mathbf{W}_{\text{rel}} = \begin{bmatrix} \frac{\partial X}{\partial t} - W_X \\ \frac{\partial Y}{\partial t} - W_Y \\ \frac{\partial Z}{\partial t} - W_Z \end{bmatrix} \tag{14}$$

Aerodynamic effects, including the balloon's natural buoyancy [10], are summarized in Eq. (15):

$$\begin{aligned}
&(m_B + m_a)\frac{\mathrm{d}^2 X_I}{\mathrm{d}t^2} \\
&\quad = (m_{\text{air}} + m_a)\frac{\partial W_X}{\partial t} - \frac{1}{2}\rho_a C_D A_B\left(\frac{\mathrm{d}X}{\mathrm{d}t} - W_X\right)|\mathbf{W}_{\text{rel}}| \\
&(m_B + m_a)\frac{\mathrm{d}^2 Y_I}{\mathrm{d}t^2} \\
&\quad = (m_{\text{air}} + m_a)\frac{\partial W_Y}{\partial t} - \frac{1}{2}\rho_a C_D A_B\left(\frac{\mathrm{d}Y}{\mathrm{d}t} - W_Y\right)|\mathbf{W}_{\text{rel}}| \\
&(m_B + m_a)\frac{\mathrm{d}^2 Z_I}{\mathrm{d}t^2} \\
&\quad = -(m_{\text{air}} + m_a)\frac{\partial W_Z}{\partial t} - \frac{1}{2}\rho_a C_D A_B\left(\frac{\mathrm{d}Z}{\mathrm{d}t} - W_Z\right)|\mathbf{W}_{\text{rel}}| - m_{\text{air}} g
\end{aligned} \tag{15}$$

The aerodynamic drag acting on the tether and the payload was neglected from the following reasons:

1) The drag force acting on the balloon is about 1000 times stronger than the drag force acting on the tether/payload.

2) The worst case of angular deviation θ_T, due to surface winds perturbing the payload, is less than 0.01 deg.

Linear Approximation

Now consider the case in which the state variables are small, and let us write the equations of motion in a linear form. The linearization assists us in viewing the system modal dynamics and is essential for the controller design. Realization of Eqs. (5) and (6) with Eqs. (10) and (12) results in the following 13 equations of motion:

$$\begin{aligned}
&(m_B + m_a + m_G + m_C)\ddot{X}_I + (m_G + m_C)\rho_B\ddot{\theta}_B + (m_G + m_C)L\ddot{\theta}_T \\
&\quad + (m_G\rho_G + m_C d)\ddot{\theta}_P + m_C\overset{\circ\circ}{\delta}_1 \\
&\quad = (m_{\text{air}} + m_a)\frac{\partial W_X}{\partial t} - \frac{1}{2}\rho_a C_D A_B(\dot{X}_I - W_X)|\mathbf{W}_{\text{rel}}|
\end{aligned} \tag{16}$$

$$\begin{aligned}
&(m_B + m_a + m_G + m_C)\ddot{Y}_I + (m_G + m_C)\rho_B\ddot{\phi}_B - (m_G + m_C)L\ddot{\phi}_T \\
&\quad - (m_G\rho_G + m_C d)\ddot{\phi}_P + m_C\overset{\circ\circ}{\delta}_2 \\
&\quad = (m_{\text{air}} + m_a)\frac{\partial W_Y}{\partial t} - \frac{1}{2}\rho_a C_D A_B(\dot{Y}_I - W_Y)|\mathbf{W}_{\text{rel}}|
\end{aligned} \tag{17}$$

$$\begin{aligned}
&(m_B + m_a + m_G + m_C)\ddot{Z}_I = (m_{\text{air}} + m_a)\frac{\partial W_Z}{\partial t} \\
&\quad - \frac{1}{2}\rho_a C_D A_B(\dot{Z}_I - W_Z)|\mathbf{W}_{\text{rel}}| + (m_B + m_G + m_C - m_{\text{air}})g
\end{aligned} \tag{18}$$

$$\begin{aligned}
&-(m_G + m_C)\ddot{Y}_I + \left(m_G + m_C + \frac{I_B}{\rho_B^2}\right)\rho_B\ddot{\phi}_B + (m_G + m_C)L\ddot{\phi}_T \\
&\quad + (m_G\rho_G + m_C d)\ddot{\phi}_P + (m_G + m_C)g\phi_B - m_c\overset{\circ\circ}{\delta}_2 = 0
\end{aligned} \tag{19}$$

$$\begin{aligned}
&-(m_G + m_C)\ddot{X}_I + \left(m_G + m_C + \frac{I_B}{\rho_B^2}\right)\rho_B\ddot{\theta}_B + (m_G + m_C)L\ddot{\theta}_T \\
&\quad + (m_G\rho_G + m_C d)\ddot{\theta}_P + (m_G + m_C)g\theta_B + m_c\overset{\circ\circ}{\delta}_1 = 0
\end{aligned} \tag{20}$$

$$\ddot{\psi}_B \cong 0 \tag{21}$$

$$\begin{aligned}
&-(m_G + m_C)\ddot{Y}_I + (m_G + m_C)\rho_B\ddot{\phi}_B + (m_G + m_C)L\ddot{\phi}_T \\
&\quad + (m_G\rho_G + m_C d)\ddot{\phi}_P + (m_G + m_C)g\phi_T - m_C\overset{\circ\circ}{\delta}_2 = 0
\end{aligned} \tag{22}$$

$$\begin{aligned}
&-(m_G + m_C)\ddot{X}_I + (m_G + m_C)\rho_B\ddot{\theta}_B + (m_G + m_C)L\ddot{\theta}_T \\
&\quad + (m_G\rho_G + m_C d)\ddot{\theta}_P + (m_G + m_C)g\theta_T + m_C\overset{\circ\circ}{\delta}_1 = 0
\end{aligned} \tag{23}$$

$$\begin{aligned}
&-\left(m_G\frac{\rho_G}{d} + m_C\right)\ddot{Y}_I + \left(m_G\frac{\rho_G}{d} + m_C\right)\rho_B\ddot{\phi}_B \\
&\quad + \left(m_G\frac{\rho_G}{d} + m_C\right)L\ddot{\phi}_T \\
&\quad + \left(m_G\left(\frac{\rho_G}{d}\right)^2 + m_C + \frac{I_{xx}^G + I_t^C}{d^2}\right)d\ddot{\phi}_P \\
&\quad + \left(m_G\frac{\rho_G}{d} + m_C\right)g\phi_P - m_C\overset{\circ\circ}{\delta}_2 - \frac{m_C g}{d}\delta_2 = 0
\end{aligned} \tag{24}$$

$$\begin{aligned}
&-\left(m_G\frac{\rho_G}{d} + m_C\right)\ddot{X}_I + \left(m_G\frac{\rho_G}{d} + m_C\right)\rho_B\ddot{\theta}_B \\
&\quad + \left(m_G\frac{\rho_G}{d} + m_C\right)L\ddot{\theta}_T \\
&\quad + \left(m_G\left(\frac{\rho_G}{d}\right)^2 + m_C + \frac{I_{yy}^G + I_t^C}{d^2}\right)d\ddot{\theta}_P \\
&\quad + \left(m_G\frac{\rho_G}{d} + m_C\right)g\theta_P + m_C\overset{\circ\circ}{\delta}_1 + \frac{m_C g}{d}\delta_1 = 0
\end{aligned} \tag{25}$$

$$\underbrace{(I_{zz}^G + I_a^C)\ddot{\psi}_P}_{\text{linear}} - \underbrace{(I_{xx}^G + I_t^C)\theta_P\ddot{\phi}_P + (I_{yy}^G - I_{zz}^G + I_t^C - I_a^C)\phi_P\ddot{\theta}_P + (I_{yy}^G - I_{xx}^G - I_{zz}^G - I_a^C)\dot{\phi}_P\dot{\theta}_P}_{\text{slightly nonlinear}} = M_\psi^P \tag{26}$$

$$\ddot{\delta}_1 = K_\delta I_{\delta_1} \tag{27}$$

$$\ddot{\delta}_2 = K_\delta I_{\delta_2} \tag{28}$$

Notice the small nonlinearity that was kept in the equation for the payload yaw. It was retained because it may be at the same order of magnitude as the small external yaw torque. An interesting possibility, which was not investigated in this work, is to try regulating the yaw via the nonlinearity with roll-pitch maneuvers. It is a challenging problem for future research.

The linear equations are rewritten in the following standard form ($\mathbf{q} \in \Re^{13}$):

$$\ddot{\mathbf{q}} = -\mathbf{M}^{-1}\mathbf{K}\mathbf{q} + \mathbf{M}^{-1}\mathbf{Q} + \mathbf{M}^{-1}\mathbf{U} \tag{29}$$

The 13×13 mass matrix $\mathbf{M}$ and the 13×13 stiffness matrix $\mathbf{K}$ can be easily constructed by inspecting Eqs. (16–28).

$\mathbf{Q}$ is a 13-element column of applied forces, for which only the first three elements are nonzero:

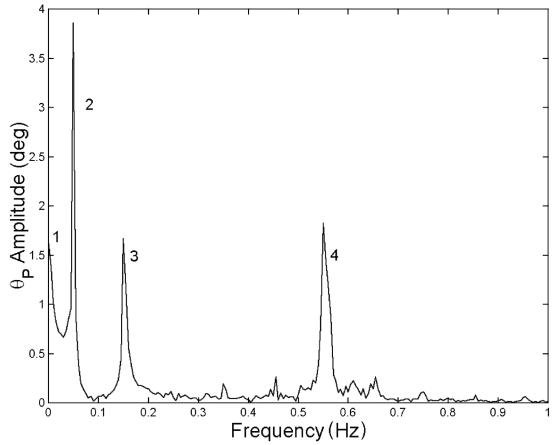

Fig. 3 Frequency spectrum of the payload pitch (without balloon damper).

$$\mathbf{Q} = \begin{bmatrix} (m_{\text{air}} + m_a)\frac{\partial W_X}{\partial t} - \frac{1}{2}\rho_a C_D A_B(\dot{X}_I - W_X)|\mathbf{W}_{\text{rel}}| \\ (m_{\text{air}} + m_a)\frac{\partial W_Y}{\partial t} - \frac{1}{2}\rho_a C_D A_B(\dot{Y}_I - W_Y)|\mathbf{W}_{\text{rel}}| \\ (m_{\text{air}} + m_a)\frac{\partial W_Z}{\partial t} - \frac{1}{2}\rho_a C_D A_B(\dot{Z}_I - W_Z)|\mathbf{W}_{\text{rel}}| + (m_B + m_G + m_C - m_a)g \\ \mathbf{0}_{11\times 1} \end{bmatrix} \tag{30}$$

$\mathbf{U}$ is a 13-element column of applied controls in which the first 11 elements are zero:

$$\mathbf{U} = \begin{bmatrix} \mathbf{0}_{11\times 1} \\ I_\delta T_{\delta_1} \\ I_\delta T_{\delta_2} \end{bmatrix} \tag{31}$$

Numerical Examples

Consider a standard atmosphere at 40 km, typical winds, and gravity waves. The surface winds were modeled as a rotating ellipsoid with frontal and side wind amplitudes of 60 and 20 kt, respectively, and a rotation period of 2 min. The vertical winds were modeled with multiple periods of 30, 60, and 120 s and with an amplitude of 2 kt. The gravity-wave model was adopted from meteorological literature [11,12], traditionally formulated as a sinusoid with a constant period and a constant amplitude. These atmospheric disturbances models are convenient for high-altitude balloons, just as the Dryden model is convenient for atmospheric flight. The gravity-wave amplitude, length, and period are 1 m/s, 10 km, and 10 min, respectively. These atmospheric disturbances are quite conservative; the test will be performed in calmer and "controlled" weather conditions. Our balloon system parameters are

$$m_B = 1600\,\text{kg}, \quad m_G = 800\,\text{kg}, \quad m_C = 1000\,\text{kg}$$
$$m_{\text{air}} = 3400\,\text{kg} \quad \text{R}_B = 66\,\text{m}, \quad \rho_B = 66\,\text{m}, \quad \text{L}_G = 1\,\text{m}$$
$$\rho_T = 70\,\text{m}, \quad \rho_G = 0.5\,\text{m}, \quad \text{L}_C = 2.3\,\text{m} \quad \text{I}_B = 2.8 \times 10^6\,\text{kg}\cdot\text{m}^2$$
$$\text{I}_{XX_G} = \text{I}_{YY_G} = 300\,\text{kg}\cdot\text{m}^2, \quad \text{I}_{t_G} = 600\,\text{kg}\cdot\text{m}^2 \quad I_\delta = 1\,\text{kg}^{-1}\cdot\text{m}^{-2}$$

The longitudinal modal response based on the preceding configuration is shown in Fig. 3 as a frequency spectrum. Four dominant frequencies are denoted: Frequency 1 reflects the balloon natural buoyancy oscillations. Frequencies 2 and 3 are related to the balloon and tether pendular motions, respectively. Frequency 4, the highest, represents the payload librations.

Introducing a damping mechanism attenuates the balloon/tether librations amplitudes and even locks their frequencies, as Fig. 4 suggests. It is a welcome result because it assists in modal stabilization, whereas the remaining mode, the payload librations, will be stabilized with active control. Note that the energy-dissipation mechanism is common in satellite applications, usually by means of viscous ring dampers. This concept has been applied (by our institution) to damp balloon oscillations. The mechanism consists of a steel ball placed on a concave glass, both inside a pressure container filled with oil. It will be mounted on top of the payload platform.

In Fig. 4, is difficult to detect the spectral component of the wind because its frequency is low relative to the system modes. Investigations concluded that the wind, rather than the initial

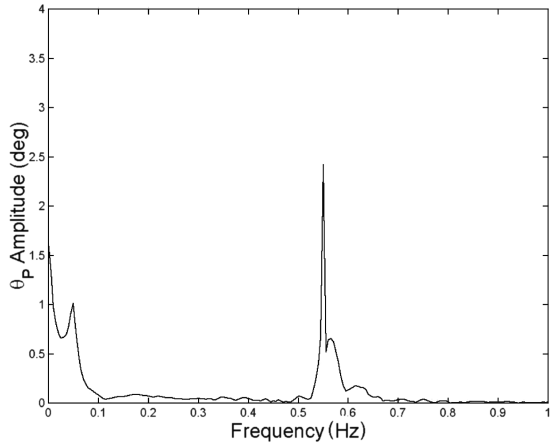

Fig. 4 Frequency spectrum of the payload pitch (with balloon damper).

conditions, is the dominant mechanism for the oscillations. It was observed that the amplitudes of the librations are in the linear domain. Accordingly, stabilization via a linear controller is a feasible approach.

Pointing Stabilization

Control Logic

The stabilization task is to bring the disturbed linear system, given by Eq. (29), from an arbitrary initial state to a required terminal state using acceptable control displacement. The terminal time is not specified; the drop is executed at the right epoch that satisfies the pointing conditions. The corresponding state vector is defined based on Eq. (7):

$$\mathbf{X} = \begin{bmatrix} q \\ \dot{q} \end{bmatrix} \in \Re^{26} \tag{32}$$

This state is associated with the linear system structure

$$\dot{\mathbf{X}} = \mathbf{A}\mathbf{X} + \mathbf{D}(\mathbf{X}, t) + \mathbf{B}\mathbf{u} \tag{33}$$

such that $\mathbf{A} \in \Re^{26\times 26}$ is the system matrix

$$\mathbf{A} = \begin{bmatrix} \mathbf{0}_{13\times 13} & \mathbf{I}_{13\times 13} \\ -\mathbf{M}^{-1}\mathbf{K} & \mathbf{0}_{13\times 13} \end{bmatrix} \tag{34}$$

$\mathbf{B} \in \Re^{26\times 2}$ is the control matrix

$$\mathbf{B} = \begin{bmatrix} \mathbf{0}_{13\times 2} \\ K_\delta \mathbf{M}^{-1} \begin{bmatrix} \mathbf{0}_{11,2} \\ \mathbf{I}_{2,2} \end{bmatrix} \end{bmatrix} \tag{35}$$

$\mathbf{D} \in \Re^{26\times 1}$ is the disturbance matrix (aerodynamic forces)

$$\mathbf{D} = \begin{bmatrix} \mathbf{0}_{13,1} \\ \mathbf{M}^{-1}\mathbf{Q} \end{bmatrix} \tag{36}$$

and $\mathbf{u} \in \Re^{2\times 1}$ is the control vector

$$\mathbf{u} = \begin{bmatrix} I_{\delta_1} \\ I_{\delta_2} \end{bmatrix} \tag{37}$$

As expected, a controllability test shows that the full state is uncontrollable. Nevertheless, because the goal is restricted to gondola pointing stabilization, we are mainly concerned with output controllability. The controllable output state vector $\mathbf{Y}$ consists of ϕ_T, θ_T, $\phi_P\theta_P$, δ_1, δ_2, and their rates. We can furthermore restrict the output state vector to ϕ_P θ_P, δ_1 , δ_2, and their rates.

A further technical step before the assignment of a control law is eliminating the redundant modes. In addition to the elimination of Z_I, ψ_B and ψ_P and $\ddot{X}_I$ and $\ddot{Y}_I$ can be eliminated as follows:

$$\ddot{X}_I = \frac{1}{M_{1,1}}\left[-M_{1,5}\ddot{\theta}_B - M_{1,8}\ddot{\theta}_T - M_{1,10}\ddot{\theta}_P - M_{1,12}\ddot{\delta}_1 + (m_{\text{air}} + m_a)\frac{\partial W_X}{\partial t} - \frac{1}{2}\rho_a C_D A_B(\dot{X}_I - W_X)|\mathbf{W}_{\text{rel}}|\right] \tag{38a}$$

$$\ddot{Y}_I = -\frac{1}{M_{2,2}}\left[M_{2,4}\ddot{\theta}_B + M_{2,7}\ddot{\theta}_T + M_{2,9}\ddot{\theta}_P + M_{2,13}\ddot{\delta}_2 + (m_{\text{air}} + m_a)\frac{\partial W_Y}{\partial t} - \frac{1}{2}\rho_a C_D A_B(\dot{Y}_I - W_Y)|\mathbf{W}_{\text{rel}}|\right] \tag{38b}$$

After substituting $\ddot{X}_I$ and $\ddot{Y}_I$ into the other equations of motion (19), (20), and (22–25), we are left with a set of eight states, all observable and controllable.

The control gain $\mathbf{G}$ was computed based on the linear quadratic regulator (LQR) algorithm [13], in which the control minimizes a weighted quadratic performance function. The optimal control gain for this LQR is related to the solution of the algebraic Riccati equation [13], and the linear control law is $\mathbf{u} = \mathbf{G}\mathbf{Y}$.

There are a variety of commercial off-the-shelf (COTS) sensors to provide the state feedback measurements. The angular orientation of the platform with respect to the vertical (the nadir) can be estimated by means of a sun-sensor/star-tracker. The typical angular measurement accuracy is of a few arc seconds with a bandwidth of 2–6 Hz. Note that a star tracker is adequate at 40 km (stars are detectable). Although this sensor is sufficient, it is possible to include an inertial navigation system that consists of three rate gyros, three orthogonal accelerometers, and possibly three magnetometers. The inertial navigation system and the sun-sensor/star-tracker are fused; the former is in the inner loop and the latter is in the outer loop. The magnetometers' role is mainly for prior estimation and backup, because their typical accuracy is only 0.1 deg, with a satisfactory bandwidth of 3 Hz. The angular inclination of the tether relative to the gondola can be measured by a rotary encoder with a precision of a

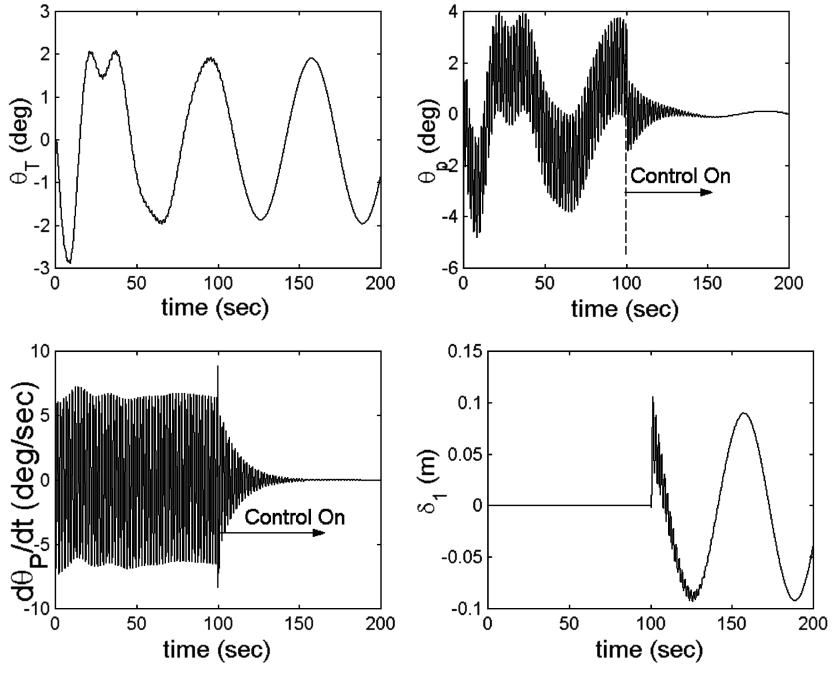

Fig. 5 Controlled pitch.

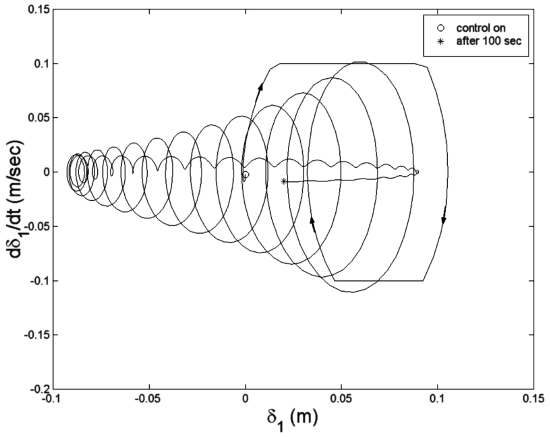

Fig. 6 Actuator longitudinal motion–phase plot.

couple of arc seconds and a count rate of 20 MHz. Information on the actuator displacement (position and velocity) at each sample time is available without estimation [14]. Because of the sensors' high performance with relation to the design requirement and to the closed-loop bandwidth, we assumed perfect measurement for this study.

Numerical Example

Numerous simulations with different initial conditions, various disturbances, and few weight matrices were run. Essentially, all scenarios were regulated with satisfactory pointing precision, acceptable control movements, and a reasonable response time. The next couple of figures demonstrate the control performance for particular weight ratios of 1:10:0:1:1:4:0:1 for $\theta_T{:}\theta_P{:}\delta_1{:}I_{\delta_1}{:}\dot{\theta}_T{:}\dot{\theta}_P{:}\dot{\delta}_1{:}\dot{I}_{\delta_1}$ and the same ratios for the equivalent lateral weights. A damper was not included to test the conservative case. Figure 5 shows the tether pitch, the payload pitch and pitch rate, and the actuator displacement for a 200-s simulation. The system is uncontrolled during the first 100 s with an initial payload pitch of 2 deg. The main excitation, however, is by the wind. Although the tether oscillations are not affected by the control action, the pitch oscillations are regulated in less than 40 s. This disturbance rejection is impressive, considering the gusty conditions.

In addition to satisfying performance, the actuator displacement stays in the acceptable tolerance. After the initial rise, it oscillates with the highest modal frequency (0.55 Hz), with low amplitude ($\sim$1 cm). The available bandwidth of COTS actuators is at least 2 Hz, sufficient for this task. Figure 6 shows a phase plot for 100 s of control action. The initial and final positions are marked by a circle and a star, respectively. Although the displacement rate reaches saturation at the first cycle, it operates within limits during the remaining time. Recall that the weight matrices are arbitrary. Increasing the control weight will relax the control agility at the expense of the performance. Conversely, reducing the control weight will improve the performance at the cost of violating the capacity of the stepper motor.

Conclusions

A dynamic model for a multibody balloon system was constructed, and the feasibility of an active control for pointing stabilization and disturbance rejection was tested. The design was verified by exciting the system via challenging atmospheric disturbances, with resulting adequate pointing regulation response and satisfactory control actions. Although we assumed perfect measurements, we do not expect a deterioration of the pointing performance when sensors are included. This is due to the expected high performance of the sensors as well as our conservative tests. It was found that a balloon dissipation mechanism assists in damping the balloon and the tether pendular motion. Possible dampers are a ring damper for damping the yaw and a special damper for damping the pendular motion. Both can be mounted on top of the payload platform. Dampers also have an important role in attenuating the elastic modes. The yaw is dynamically decoupled (in the linear sense) and may be controlled by a reaction wheel. In any case, the regulation of the yaw is not a tight design requirement and probably can be tolerated by dampers, with no need for active control. In general, there are approximations in modeling the dynamics and uncertainties in modeling the atmospheric disturbances. Nevertheless, this imprecision can be considered as a form of internal disturbance exciting the gondola dynamics. As long as the unmodeled frequency spectrum is not too high relative to the modeled frequency spectrum (indeed, the tether longitudinal flexible-mode vibration frequency is less than 0.5 Hz), it is believed that the proposed dampers and controller will reject the unmodeled disturbances.

Acknowledgments

Support for this work was provided by NASA's John H. Glenn Research Center at Lewis Field through grant NAG3-2881 to the Smithsonian Astrophysical Observatory. The author would also like to thank Roger Hain from the Smithsonian Astrophysical Observatory for his helpful comments.

References

[1] Shapiro, I. I., Lorenzini, E. C., Ashenberg, J., Cheimets, P. N., Iafolla, V., Lucchesi, D. M., Nozzoli, F., Santoli, F., and Glawhow, S., "Testing the Principle of Equivalence in an Einstein Elevator," *International Journal of Modern Physics D* (to be published).

[2] Ashenberg, J., and Lorenzini, E. C., "Analytical Formulation of a Complex Mutual Gravitational Field," *Classical and Quantum Gravity*, Vol. 21, No. 8, 2004, pp. 2089–2100. doi:10.1088/0264-9381/21/8/012

[3] Ashenberg, J., and Lorenzini, E. C., "Gravitational Torque Frequency Spectral Analysis for Einstein Elevator Experiment," *Classical and Quantum Gravity*, Vol. 24, 2007, pp. 4251–4268. doi:10.1088/0264-9381/24/17/001.

[4] Quadrelli, M. B., Cameron, J. M., and Kerzhanovich, V., "Multibody Dynamics of Parachute and Balloon Flight System for Planetary Exploration," *Journal of Guidance, Control, and Dynamics*, Vol. 27, No. 4, July–Aug. 2004, pp. 564–571.

[5] Lemke, L. G., Powell, J. D., and He, X., "Attitude Control of Tethered Spacecraft," *Journal of the Astronautical Sciences*, Vol. 35, No. 1, 1987, pp. 41–55.

[6] Ashenberg, J., "Active Gravity Gradient Stabilization of a Satellite in Elliptic Orbits," *Acta Astronautica*, Vol. 45, No. 10, Nov. 1999, pp. 619–627. doi:10.1016/S0094-5765(99)00127-7

[7] Hughes, P. C., *Spacecraft Attitude Dynamics*, Wiley, New York, 1986, pp. 522–534.

[8] Landau, L. D., and Lifschitz, E., *Fluid Mechanics*, Pergamon, Oxford, 1959, pp. 33–44.

[9] Azinheira, J. R., Carneiro de Paiva, E., and Bueno, S. S., "Influence of Wind Speed on Airship Dynamics," *Journal of Guidance, Control, and Dynamics*, Vol. 25, No. 6, 2002, pp. 1116–1124.

[10] Massman, W. J., "On the Nature of Vertical Oscillations of Constant Volume Balloons," *Journal of Applied Meteorology*, Vol. 17, Sept. 1978, pp. 1351–1356. doi:10.1175/1520-0450(1978)017<1351:OTNOVO>2.0.CO;2

[11] Hanna, S. R., and Hoecker, W. H. "The Response of Contant-Density Balloons to Sinusoidal Variations of Vertical Wind Speed," *Journal of Applied Meteorology*, Vol. 10, June 1971, pp. 601–604. doi:10.1175/1520-0450(1971)010<0601:TROCDB>2.0.CO;2

[12] Nastrom, G. D., "The Response of Superpressure Balloons to Gravity Waves," *Journal of Applied Meteorology*, Vol. 19, Aug. 1980, pp. 1013–1019. doi:10.1175/1520-0450(1980)019<1013:TROSBT>2.0.CO;2

[13] Bryson, E. B., and Ho, Y. C., *Applied Optimal Control*, Hemisphere, New York, 1975, pp. 148–152.

[14] Kline-Schoder, R. J., and Powell, J. D., "Precision Attitude Control for Tethered Satellites," *Journal of Guidance, Control, and Dynamics*, Vol. 16, No. 1, 1993, pp. 168–174.